Research Article

Evaluating the Impact of Nano Silver and Zinc Oxide Quantum Dots on Pulmonary and Cardiac Lesions in Chicks Following *E. coli* Infection

Mohammed Abdeldayem Mohammed Afifi[1]*, Shawky Ahmed Moustafa[2], Aziza Abd El-Fattah Amin[2], Sawsan Sami Mesalam El-Basuni[3] and Mohamed Mahmoud Salem Gaballa[4]

[1]Faculty of Veterinary Medicine, Benha University, Egypt; [2]Department of Pathology, Faculty of Veterinary Medicine, Benha University, Egypt; [3]Department of Avian and Rabbit Diseases, Faculty of Veterinary Medicine, Benha University, Egypt; [4]Department of Pathology, Faculty of Veterinary Medicine, Benha University, Egypt.

Abstract | *E. coli* infections, particularly those caused by avian pathogenic *E. coli* (APEC) strains such as O78, remain a major concern in poultry health. The increasing prevalence of antibiotic-resistant strains due to the overuse of conventional antibiotics has made treating such infections increasingly difficult. Nanotechnology provides promising alternative therapies. Accordingly, this study investigates the potential of silver nanoparticles (Ag NPs) and zinc oxide quantum dots (ZnO QDs) in preventing and treating cardiopulmonary lesions caused by *E. coli* in broiler chicks. In this study, 80 one-day-old Specific Pathogen-Free (SPF) broiler chicks were divided into eight groups (10 chicks per group), Group 1 is negative control, Group 2 received only Ag NPs, Group 3 received only ZnO QDs. The remaining five groups were challenged with *E. coli* O78 via oral gavage. Group 4 was untreated post-infection. Groups 5 and 6 received preventive treatment with (Ag NPs or ZnO QDs) before infection with *E. coli*. Groups 7 and 8 received therapeutic treatment with (Ag NPs or ZnO QDs) after *E. coli* infection. Results included clinical signs and post-mortem findings and histopathological evaluations of lung and heart tissues. The *E. coli* group showed clinical symptoms, including lethargy, anorexia, open-mouth breathing, diarrhea, and ruffled feathers. On necropsy, this group revealed dark red patches and hemorrhage in the lungs, along with fibrinous deposits on the pericardium. Microscopically, the *E. coli* group displayed severe lesions in the lung, such as alveolar congestion, hemorrhage into the alveolar spaces, thickened alveolar septa with intense inflammation, distended bronchiolar lumens, and damaged blood vessel endothelium with perivascular edema and inflammation. Additionally, necrosis, extensive inflammation, loss of striation, and hemorrhage were observed in the heart. High average lesion scores in the histopathological scoring confirmed this severe damage. In contrast, chicks treated with Ag NPs and ZnO QDs showed only mild clinical signs and gross lesions, along with a significant reduction in lesion severity, confirmed by histopathological scoring. The study concluded that both Ag NPs and ZnO QDs significantly mitigated the severity of pulmonary and cardiac lesions caused by *E. coli* infection.

Received | February 16, 2025; **Accepted** | March 25, 2025; **Published** | April 26, 2025
***Correspondence** | Mohammed Abdeldayem Mohammed Afifi, Faculty of Veterinary Medicine, Benha University, Egypt; **Email:** mohammed_abdeldaim@yahoo.com
Citation | Afifi, M.A.M., S.A. Moustafa, A.A.E-F. Amin, S.S.M. El-Basuni and M.M.S. Gaballa. 2025. Evaluating the impact of nano silver and zinc oxide quantum dots on pulmonary and cardiac lesions in chicks following *E. coli* infection. *Advanced Analytical Pathology,* 1: 52-63.
DOI | https://dx.doi.org/10.17582/journal.aap/2025/1.52.63
Keywords | Broiler chicks, *E. coli*, Nanoparticles, Silver, Zinc oxide

Copyright: 2025 by the authors. Licensee ResearchersLinks Ltd, England, UK.
This article is an open access article distributed under the terms and conditions of the Creative Commons Attribution (CC BY) license (https://creativecommons.org/licenses/by/4.0/).

Introduction

Colibacillosis in poultry is a major issue, causing high rates of morbidity and mortality among birds and resulting in significant economic losses (Pourbakhsh *et al.*, 1997). It is a complex, multisystemic disease that affects several organs, causing lesions in the air sacs, pericardium, peritoneum, joints, oviducts, bones, and yolk sacs (Shah *et al.*, 2019).

The respiratory system, specifically the lungs, serves as a primary route for *E. coli* infections in poultry. Inhalation of dust, in which *E. coli* can survive for extended periods, introduces the pathogen into the lungs (Paudel *et al.*, 2021). Once inside the lungs, *E. coli* is more likely to colonize because of the relatively weak local immune defense mechanisms in the lungs of poultry. Unlike mammals, poultry lungs have fewer resident macrophages in their lung tissue and rely on recruitment of macrophages to the infection site when needed, which makes them particularly vulnerable to infections (Pourbakhsh *et al.*, 1997). In addition to the lungs, the heart is another critical organ affected by *colibacillosis*. Avian pathogenic *E. coli* (APEC) can cause septicemia, leading to the accumulation of bacterial colonies in cardiac tissue (Stordeur *et al.*, 2002). This results in the development of various lesions in the heart (Abd El-Ghany and Madian, 2011).

Various strains of *E. coli* isolated from poultry have developed multidrug resistance, mainly due to the overuse of antibiotics in poultry farming over many years. This misuse has made traditional antibiotics less effective in controlling *E. coli* infections. Consequently, this exacerbating issue poses a significant health risk to poultry and humans (Mellata, 2013).

In response to this growing issue, nanotechnology has emerged as a promising and innovative alternative in combating multidrug-resistant bacterial infections. Certain nanoparticles have demonstrated potent antimicrobial properties in both *in vitro* and *in vivo* studies. Additionally, they can be used synergistically with antibiotics to enhance their effectiveness in treating infections (Abreu *et al.*, 2023). Among these, silver nanoparticles have been used in many different applications due to their unique size and distinctive properties at the nanoscale, which differ from those at the bulk scale. In particular, significant research has focused on their antimicrobial effectiveness, as Ag NPs have demonstrated remarkable potential in combating a wide range of pathogens, including multidrug-resistant bacteria (Bruna *et al.*, 2021). Furthermore, zinc oxide (ZnO) has been used as a feed additive in poultry to promote growth, as Zinc is considered to be a vital trace element involved in many physiological functions in poultry (Fatima *et al.*, 2024). Moreover, ZnO has been studied for its antimicrobial properties in different forms, including nanoparticles and quantum dots, due to their unique size and biocompatibility (Jin *et al.*, 2009; Gharpure and Ankamwar, 2020). The application of Ag NPs and ZnO QDs in veterinary medicine presents a novel strategy for controlling bacterial infections in chicks. Although these nanomaterials show promise *in vitro* studies, there is insufficient *in vivo* research evaluating their protective and therapeutic efficacy in controlling *E. coli* infections, particularly in broilers. Consequently, this study investigates the potential of Ag NPs and ZnO QDs in preventing and treating cardiopulmonary lesions caused by *E. coli* in broiler chicks.

Materials and Methods

Nanoparticles

Silver nanoparticles (Ag NPs): Silver nanoparticles (Ag NPs) were synthesized using a reduction method in which silver nitrate ($AgNO_3$) was reduced by chitosan, which functioned as both a reducing agent and stabilizer. The synthesis followed the protocol outlined by Wei *et al.* (2009), resulting in stable Ag NPs suitable for experimental purposes. Ag NPs used in this study was a deep yellowish-brown suspension, with UV–vis spectroscopy confirming nanoparticle formation (surface plasmon resonance (SPR) band was at approximately 405 nm), and Transmission Electron Microscopy (TEM) indicating spherical particles averaging 12 nm.

Zinc oxide quantum dots (ZnO QDs): Zinc oxide quantum dots (ZnO QDs) were prepared using a sol-gel method. Zinc acetate and potassium hydroxide (KOH) served as the precursor materials, and 3-aminopropyltriethoxysilane (APTES) was used for surface modification. The synthesis followed the methodology described by Li *et al.* (2021), ensuring the production of stable and biocompatible ZnO QDs. The ZnO QDs used in this study were a white to yellow powder, with XRD showing an organized crystalline structure and TEM revealing spherical

particles averaging 10 nm.

Ethical approval and animal management

The study was approved by the Scientific Research Ethical Committee of the Faculty of Veterinary Medicine, Benha University (BUFVTM 08-01-24). Eighty-one-day-old Specific Pathogen-Free (SPF) broiler chicks were obtained from Nile S.P.F Company, Faiyum, Egypt. The chicks were housed under controlled conditions at the Research Center for Experimental Animals, Faculty of Veterinary Medicine, Benha University, where temperature and humidity were regulated. The birds had *ad libitum* access to water and feed, and their diet was adjusted as needed to meet age-appropriate nutritional requirements.

Experimental design

Following a one-week acclimatization period, the chicks were randomly allocated into eight experimental groups, each consisting of 10 chicks. Table 1 outlines the protective and treatment protocols, including dosages, administration periods, and *E. coli* O78 challenge conditions. The challenge strain, *E. coli* O78, was administered orally via crop gavage, following the protocol of Abd El-Tawab *et al.* (2015). Silver nanoparticles (Ag NPs) were administered at a dose of 0.5 mg/kg and Zinc oxide quantum dots (ZnO QDs) at a dose of 80 mg/kg in accordance with the methods described by Hassanen *et al.* (2021) and Li *et al.* (2021).

Preparation, isolation, and re-isolation of E. coli isolate

Isolation of *E. coli* isolate: An avian pathogenic *Escherichia coli* (APEC) strain was obtained from the Bacterial Strain Bank at the Animal Health Research Institute (AHRI), Cairo, Egypt. This strain was previously isolated from broiler cases of colisepticemia associated with high mortality rates. It was identified and serotyped as *E. coli* O78 (Ibrahim *et al.*, 2024). Prior to inoculation, the *E. coli* O78 strain was cultured aerobically in nutrient broth at 37°C for 24 hours, and the bacterial suspension was adjusted to a concentration of 1×10^8 CFU/ml.

Bacterial re-isolation: Homogenized tissue samples from the lung and heart were incubated aerobically in nutrient broth at 37°C for 24 hours and then cultured on Eosin-methylene blue (EMB) agar. The resulting colonies were identified and serotyped following the protocol outlined by Ibrahim *et al.* (2024), confirming the persistence of *E. coli* O78 in infected birds.

Sacrifice and sample collection

Two sacrifices were conducted during the experiment: one on day 19 and another on day 22 post infection. For the first sacrifice, five birds from each group were randomly selected. The remaining birds were sacrificed on day 22. During each sacrifice, a gross examination of the air sacs, lungs, and hearts was performed. Additionally, tissue samples from the lungs and hearts were collected for histopathological evaluation.

Table 1: *Detailed overview of the protective and treatment protocols, specifying dosage levels, administration durations, and conditions for the E. coli O78 challenge.*

Group	Treatment	Dosage (mg/kg bw)	Administration period	Challenge
Control	None	-	-	-
Silver nanoparticles (Ag NPs)	Ag NPs	0.5	Days 8 to 22	-
Zinc Oxide quantum dots (ZnO QDs)	ZnO QDs	80	Days 8 to 22	-
E. *coli*	None	-	-	Infected with 1×10^8 CFU/ml of *E. coli* O78 on day 14
Silver prevented group (Ag NPs prevented)	Ag NPs	0.5	Days 8 to 22	Challenged with 1×10^8 CFU/ml of *E. coli* O78 on day 14
Zinc Oxide prevented group (ZnO QDs prevented)	ZnO QDs	80	Days 8 to 22	Challenged with 1×10^8 CFU/ml of *E. coli* O78 on day 14
Silver Treated (Ag NPs treated)	Ag NPs	0.5	Days 16 to 22	Challenged with 1×10^8 CFU/ml of *E. coli* O78 on day 14
Zinc Oxide Treated (ZnO QDs treated)	ZnO QDs	80	Days 16 to 22	Challenged with 1×10^8 CFU/ml of *E. coli* O78 on day 14

Histopathological examinations

Tissue preparation: Lung and heart tissue samples were collected from all groups on day 19 and day 22. Tissue processing involved fixation in 10% formalin, followed by dehydration using ascending ethyl alcohol concentrations (70%, 90%, and absolute ethyl alcohol). Clearing was done with xylene. The tissue was then embedded in paraffin, trimmed, and sectioned to a 5 µm thickness using a microtome. The slides were stained with hematoxylin and eosin (H and E) (Bancroft and Layton, 2019). The stained slides were examined microscopically to assess pathological changes.

Histopathological scoring of lung injury: A scoring system was implemented to assess the severity of lung lesions based on HandE-stained sections. The system followed the criteria established by Mateos-Hernández *et al.* (2020), with scores ranging from 0 to 3: score (0) no leukocyte infiltration; clear peribronchial regions with no lumen stenosis; score (1) leukocyte infiltration around peribronchial regions, without lumen stenosis; score (2) focal leukocyte infiltration; peribronchial lumen not visible; score (3) multifocal inflammatory nodules, indicating significant inflammation.

Histopathological scoring of heart damage: Heart tissue damage was scored according to the method described by Chen *et al.* (2022). The scoring criteria for myocardial damage included the following: Score (1) slight granular degeneration; score (2) vacuolar degeneration; score (3) capillary congestion; score (4) inflammatory infiltration and necrosis.

Data analysis

Average scores for histopathological changes in lung and heart tissues were calculated and presented graphically. Charts were generated to visualize the average scoring trends across the experimental groups, providing an overview of the severity of lesions in response to the treatments.

Results

Clinical signs

The clinical signs observed in the *E. coli* group included lethargy, loss of appetite, gasping, brown diarrhea, and ruffled feathers. Notably, these symptoms were milder in the prevented and treated groups and absent in the control groups.

Gross lesions

Post-mortem examination of the control group revealed no gross lesions (Figure 1A, D). In contrast, the *E. coli* group exhibited marked cardiopulmonary lesions, including dark red patches (Figure 1B), hemorrhage in the lung (Figure 1C), and fibrinous deposits on the pericardium in the heart (Figure 1E). Other preventive or therapeutic groups showed mild cardiopulmonary lesions compared to the *E. coli* group.

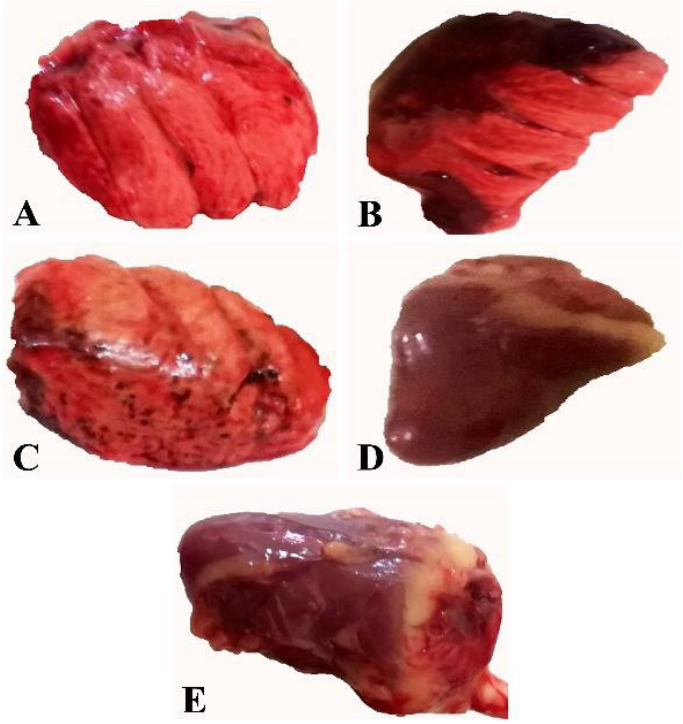

Figure 1: *Macroscopic view of the lungs and heart. A: Lung of the control group appears normal. B: The E. coli group is showing dark red patches. C: E. coli group showing hemorrhage. D: The heart of the control group appears normal. E: E. coli group revealing fibrinous deposits on the pericardium.*

Histopathology of the lungs

Histopathological analysis of lung and heart tissues across experimental groups showed distinct dissimilarities in histopathological lesions. The lung of the control group tissue appeared normal (Figure 2A, C), with clear air capillaries, thin alveolar septa, and no evidence of inflammation or structural damage. The parabronchi maintained intact epithelial linings, and the vascular structures were unremarkable.

Meanwhile, the lung sections obtained from the *E. coli* group showed significant pathological alterations as represented in the first sacrifice (Figure 2D-F) and second sacrifice (Figure 2J-L). Notably, the lesions

were more severe in the second sacrifice than in the first sacrifice. There was marked alveolar congestion with widespread hemorrhage into the alveolar spaces. With thickened alveolar septa admixed with intense infiltration of inflammatory cells, predominantly heterophils. Degeneration and desquamation of the alveolar epithelium were prominent, with areas of alveolar collapse and emphysema. Distension of the bronchial and bronchiolar lumen with edematous fluid admixed with inflammatory cells, mucus, and cellular debris. Blood vessels exhibited endothelial damage with perivascular edema and inflammatory infiltrates.

Mild alterations were observed in the Ag NPs group at both sacrifices (Figure 2B, H), including occasional thickening of the alveolar septa and mild pulmonary capillary congestion. There was limited inflammatory cell infiltration, and the bronchiolar epithelium remained largely intact with no significant fibrosis or emphysema.

Interestingly, moderate histological changes were detected in the Ag NPs prevented group as shown in (Figure 3A, C) with thickened alveolar septa and moderate infiltration of macrophages and lymphocytes were observed. Mild interstitial congestion and edema were noted, and the bronchioles showed minor hyperplasia. Early signs of fibrosis were observed, but the alveolar architecture remained discernible. The second sacrifice revealed a reduction in lesion severity compared to the first.

Meanwhile, at 19 and 22 days, mild congestion and edema were noted in the Ag NPs-treated group (Figure 3B, D), with less severe inflammation compared to the CP group. Alveolar spaces remained largely clear, with mild thickening of the alveolar septa due to macrophage infiltration. The bronchioles showed mild epithelial regeneration, with minimal luminal narrowing and decreased mucus accumulation.

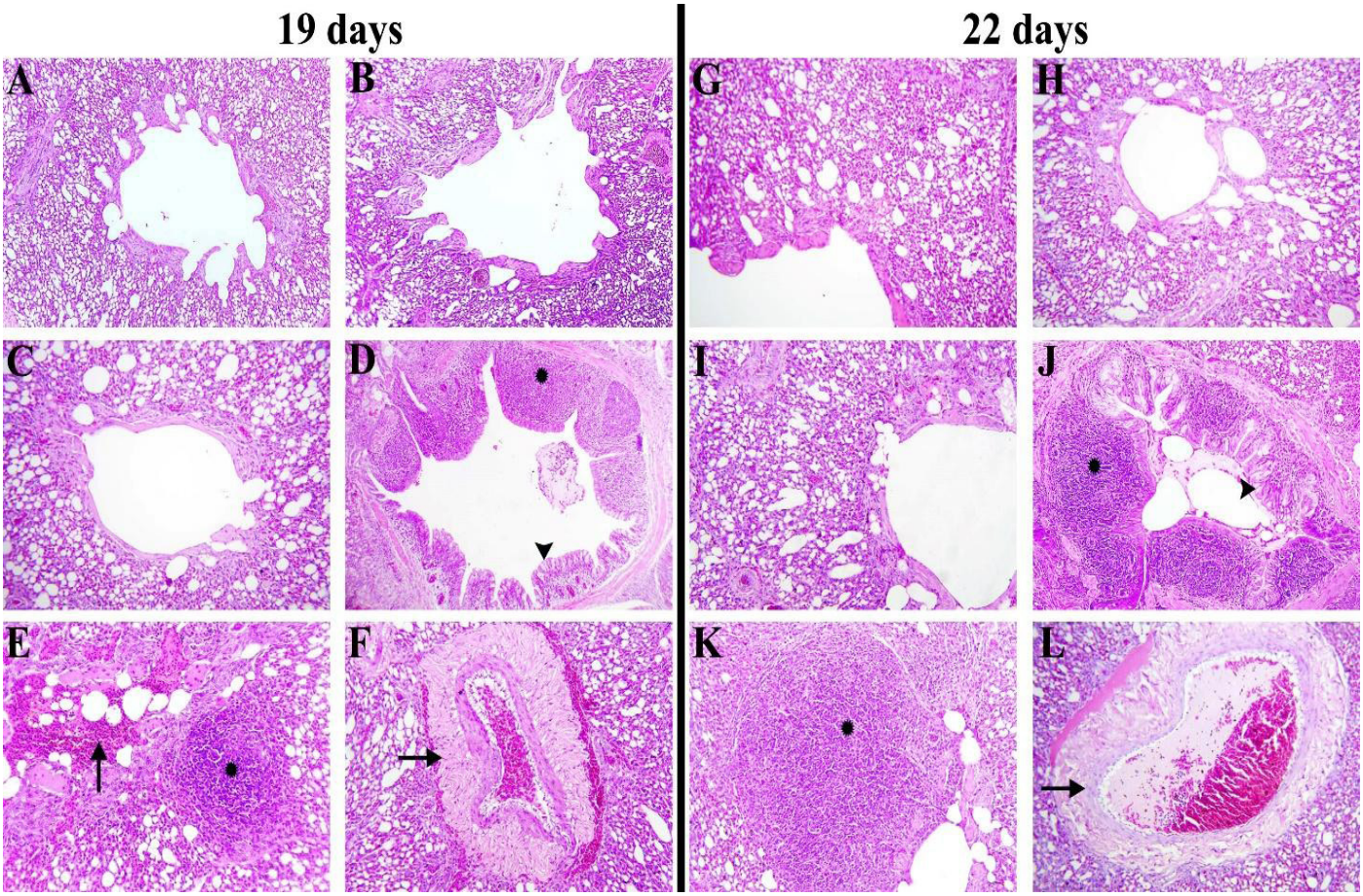

Figure 2: *Photomicrographs of lung tissue sections stained with H and E (x200) illustrating histopathological changes across various experimental groups at 19 days (A- F) and 22 days (G- L). The control group showed a normal histological structure of the lung (A and G). Ag NPs group displaying mild interstitial congestion (B and H). ZnO QDs group revealing mild edema in the air capillaries (C and I). E. coli group exhibiting severe parabronchial constriction and inflammatory cell infiltration (asterisk) (D and J), extensive lymphocytic infiltration (asterisk) with extravasated RBCs (arrow) (E and K), and endothelial injury, vascular congestion, and perivascular hemorrhage (arrows) (F and L).*

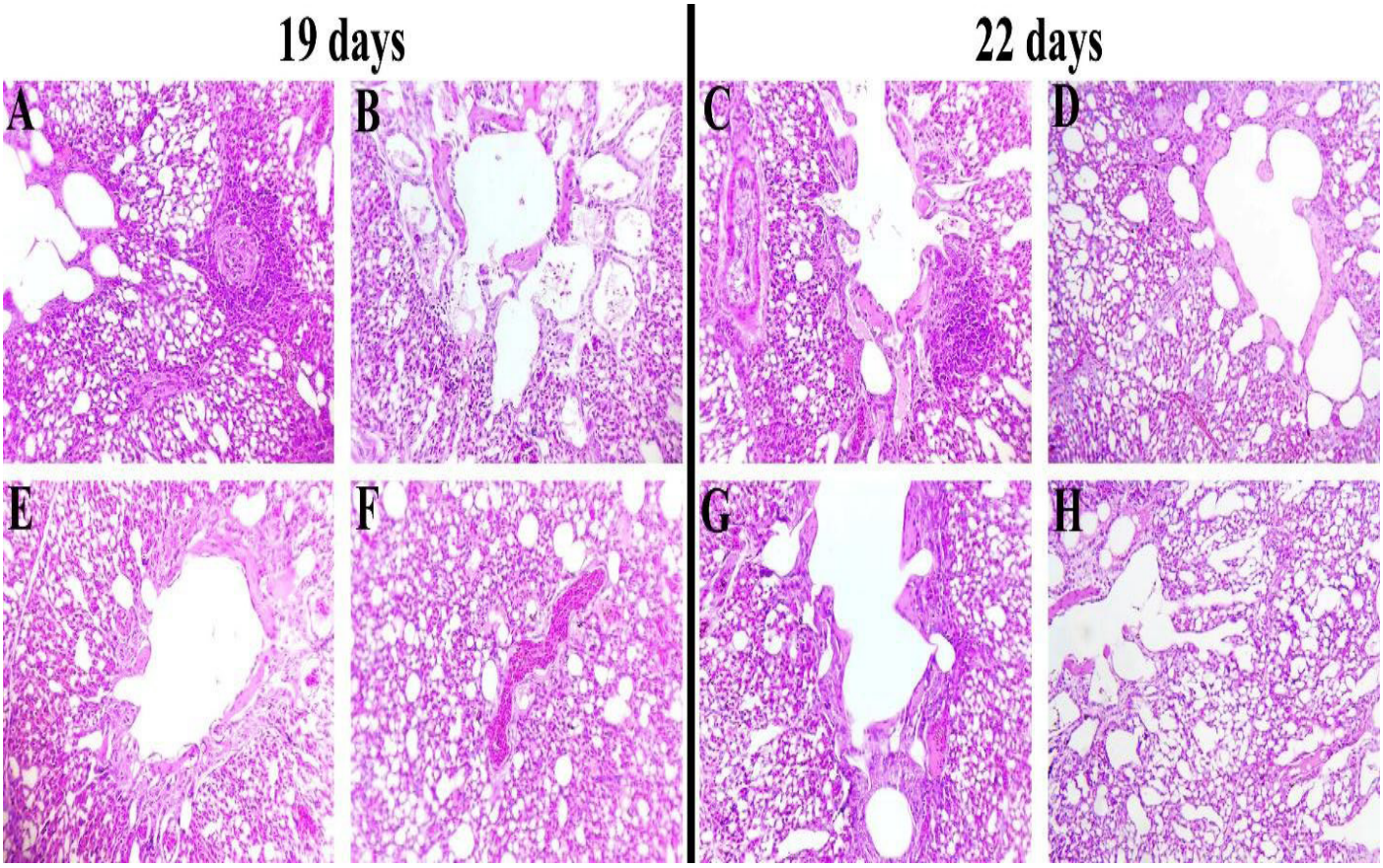

Figure 3: *Photomicrographs of lung sections stained with H and E (x200) from the Ag NPs prevented, Ag NPs treated groups at 19 days (A and B) and 22 days (C and D), and ZnO QDs prevented and ZnO QDs treated groups at 19 days (E and F) and 22 days (G and H). The Ag NPs prevented group showing moderate inflammatory cell infiltration (A and C). The Ag NPs treated group exhibited mild inflammatory cell infiltration (B and D). The ZnO QDs prevented the group from displaying mild histopathological changes (E and G). The ZnO QDs treated group showed nearly normal histological structure (F and H).*

On days 19 and 22, the lung sections of the ZnO QDs group appeared nearly normal (Figure 2C, I), with thin alveolar septa, clear alveolar spaces, and minimal pulmonary vessel congestion. There was no significant inflammatory infiltration, and the bronchioles maintained healthy epithelial linings.

Various histological changes were observed in the ZnO QDs prevented group (Figure 3E, G), including moderate infiltration of inflammatory cells, mild septal thickening, and slight interstitial edema at both sacrifices. The bronchiolar epithelium showed mild hyperplasia, with occasional luminal narrowing due to inflammatory exudates.

In the ZnO QDs treated group (Figure 3F, H), very mild histological changes were observed, including minimal inflammatory cell infiltration and slight thickening of the alveolar septa. The alveolar spaces were clear, and the bronchiolar epithelium showed only minor hyperplasia with no luminal obstruction. Notably, histological alterations were milder in the second sacrifice than in the first sacrifice.

Histopathological examination of the heart

Histological examination of the heart tissues also revealed notable differences between the groups. The heart tissue of the control group showed normal histological structure (Figure 4A, C). Myocardial fibers were well-organized, and there were no vascular abnormalities.

In *the E. coli group,* at the first sacrifice (Figure 4D, F) and second sacrifice (Figure 4J, L), severe cardiac lesions were present, including marked myocardial necrosis, extensive inflammatory cell infiltration, and significant interstitial edema. The myocardium exhibited widespread degeneration and loss of normal tissue architecture in association with multiple areas of hemorrhage. The second sacrifice exhibited a marked increase in lesion severity compared to the first sacrifice.

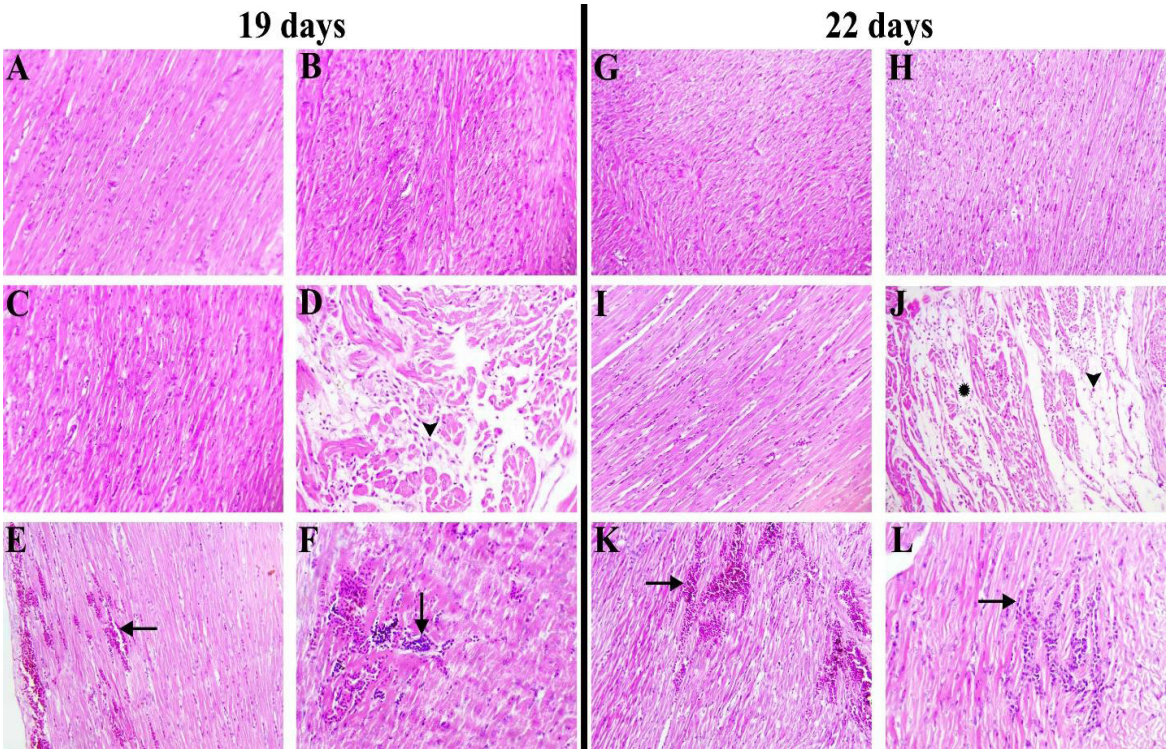

Figure 4: *Photomicrographs of heart tissue sections stained with H and E (x200) demonstrating the histopathological findings in the Control, Ag NPs, ZnO QDs, and E. coli groups at 19 days (A- F) and 22 days (G- L). The control group revealed a normal histological structure (A and G). The Ag NPs group showed no histopathological alterations (B and H). The ZnO QDs group displaying preserved cardiac tissue architecture (C, I). The E. coli group showing extensive disruption and degeneration of cardiac fibers (arrowheads) (D and J), hemorrhage (arrows) (E and K), and myocyte injury with pyknotic nuclei and inflammatory cell infiltration (arrows) (F and L).*

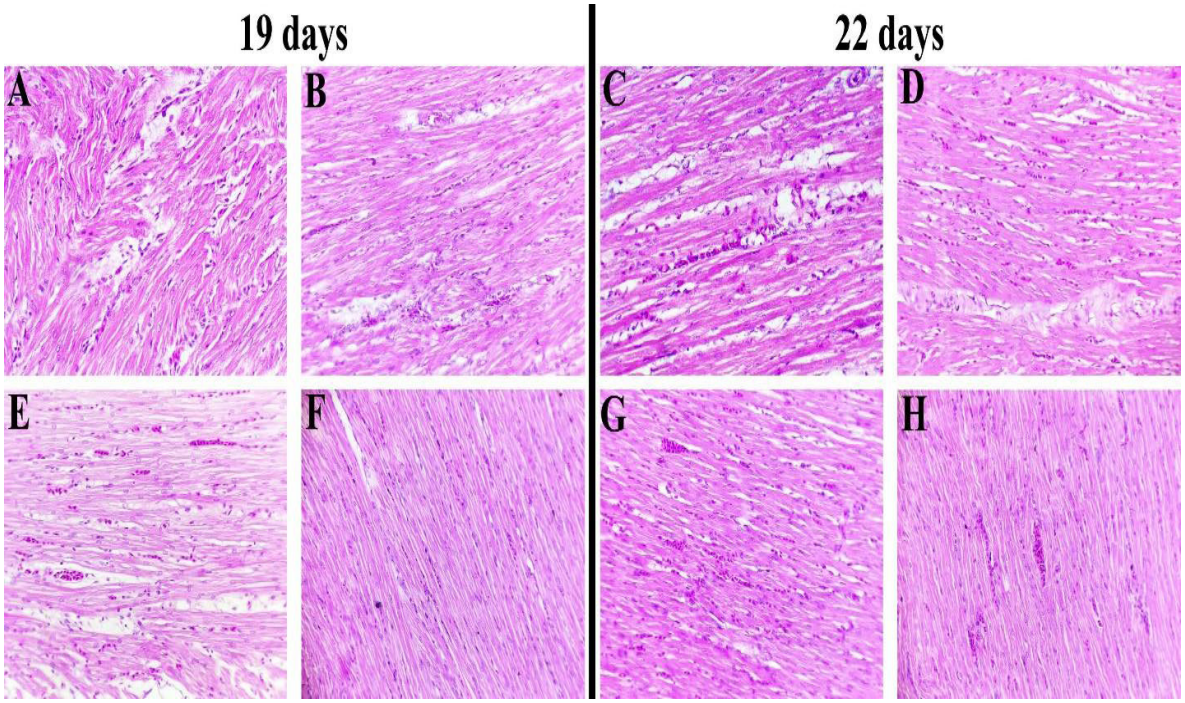

Figure 5: *Photomicrographs of heart sections stained with H and E (x200) from the Ag NPs prevented, Ag NPs treated groups at 19 days (A and B) and 22 days (C and D), and ZnO QDs prevented, and ZnO QDs treated groups at 19 days (E and F) and 22 days (G and H). The Ag NPs prevented group showing moderate degeneration and disruption of myofibers (A and C). The Ag NPs treated group revealed mild disruption and edema (B and D). The ZnO QDs prevented the group from displaying extravasated RBCs (E and G). The ZnO QDs treated group showed nearly normal histological structure (F and H).*

On days 19 and 22, mild cardiac alterations were observed in the Ag NPs group, including slight interstitial edema and occasional infiltration of inflammatory cells (Figure 4B, H). Myocardial fibers remained largely intact, with no significant necrosis or fibrosis.

At both sacrifices, moderate inflammatory infiltration was noted in the myocardium in the Ag NPs-prevent group (Figure 5A, C), with mild interstitial edema. Myocardial fibers showed early signs of degeneration, but the tissue architecture was largely preserved.

In the Ag NPs treated group at both sacrifices, mild inflammatory changes were present, with limited interstitial edema and minimal myocardial degeneration (Figure 5B, D). The overall myocardial structure was preserved, and no significant necrosis was observed.

On days 19 and 22, the heart tissues of the ZnO QDs group appeared histologically normal (Figure 5C, I), with no signs of inflammation or degeneration. The myocardial fibers were well-organized, and there was no evidence of interstitial edema or fibrosis.

Mild inflammatory cell infiltration and interstitial edema were observed in the myocardium of the ZnO QDs-prevent group at both sacrifices (Figure 5E, G). The myocardial fibers remained largely intact, with no significant necrosis or degeneration.

Very mild histological changes were noted in the ZnO QDs Treated group (Figure 5F, H), including slight inflammatory infiltration and minimal interstitial edema. The myocardial fibers showed no signs of significant degeneration or necrosis, and the tissue architecture remained well-preserved.

Histopathological evaluation

Figures 6 and 7 represent the average scores of microscopic lesions in the lung and heart of the experimental groups at both sacrifice points (day 19 and day 22). The histopathological scoring revealed varying levels of tissue injury and healing patterns across the groups. The control group achieved the lowest average scores (0.2) in lung and heart at both sacrifices, as it showed a healthy tissue pattern and provided a standard for comparison. In contrast, the *E. coli* group exhibited the most severe histopathological changes with the highest average scores in both lung (2.6 and 2.8) and heart (3.4 and 3.6). The protective and therapeutic groups treated with Ag NPs and ZnO QDs displayed different degrees of Mitigation of cardiopulmonary lesions. Additionally, the Ag NPs and ZnO QDs groups had low average scores, indicating mild pathological changes compared to the *E. coli* group.

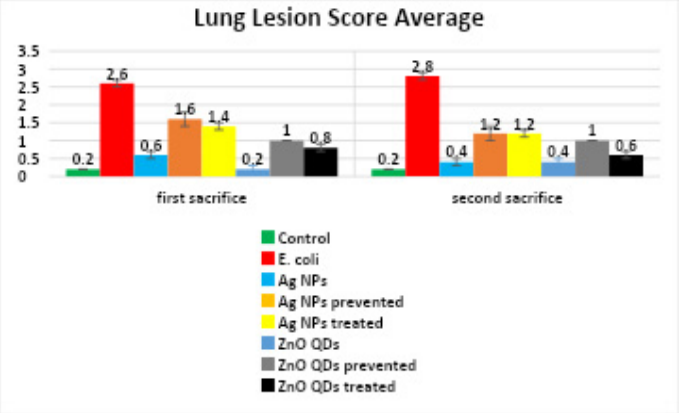

Figure 6: *Bar chart representing the average scores of histopathological lung lesions in experimental groups.*

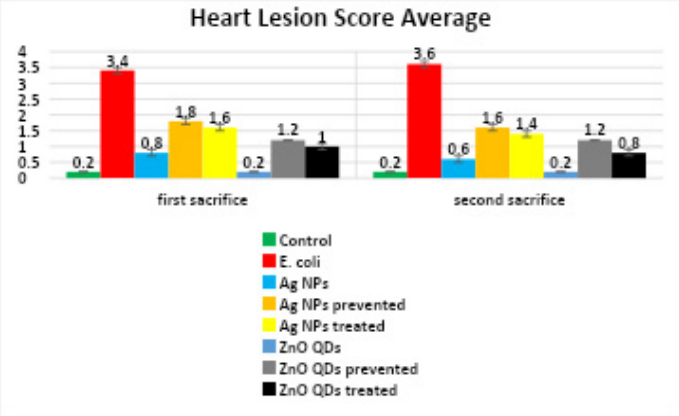

Figure 7: *Bar chart representing the average scores of histopathological heart lesions in experimental groups.*

Discussion

Colibacillosis is a serious poultry disease that appears when certain strains of *Escherichia coli*, typically considered part of the normal digestive microflora in chickens, invade other internal organs. Avian pathogenic *E. coli* (APEC) is the cause of colibacillosis and can lead to substantial financial losses. The pathogenesis of *E. coli* infection, particularly avian pathogenic *Escherichia coli* (APEC), remains poorly elucidated. However, bacteremia is widely acknowledged as a pivotal factor in the disease's progression (Leitner and Heller,1992). While the exact natural route of infection is not clearly defined, both the oral and respiratory pathways are believed

to be significant entry points for APEC (Dziva and Stevens, 2008). In fact, the management of colibacillosis has become increasingly challenging due to the ability of APEC to develop resistance genes against traditional antibiotics, resulting in a significant decrease in the efficacy of these conventional antibiotics (El-Shaer *et al.*, 2023). Therefore, this study aimed to evaluate the protective and therapeutic effects of silver nanoparticles and zinc oxide quantum dots in mitigating lesions caused by *E. coli* infection.

In this study, we observed numerous histopathological changes with various severity levels among the experimental groups. The lung tissues obtained from the *E. coli* infected group showed the most drastic microscopic changes, including congestion, hemorrhage, thickened alveolar septa, and intense inflammatory cell infiltration. Additionally, bronchioles exhibited significant inflammation and edema, while blood vessels presented with endothelial proliferation and congestion, accompanied by perivascular edema and inflammatory infiltrates. These findings are in agreement with those previously described by Singh *et al.* (2024). These histopathological alterations can be attributed to the inflammatory response triggered by bacterial infection. When bacteria invade the lung tissue, macrophages recognize the bacterial cells and act quickly by performing phagocytosis to eliminate them. This response leads to attracting leucocytes to the affected areas. Heterophils are the first cells to be recruited, moving from the bloodstream to the infected tissue; however, if colonies of the *E. coli* remain in the infected tissue, inflammation can cause lung injury and pulmonary physiological processes. Later, monocytes arrive at the infection site, further contributing to bacterial elimination and tissue repair (Guabiraba and Schouler, 2015). Furthermore, in the heart, there was evidence of myocardial necrosis, pronounced infiltration of inflammatory cells, and substantial interstitial edema. The myocardium showed widespread degeneration with a disrupted tissue architecture, along with hemorrhage. Similar results were previously observed by Amen *et al.* (2023).

Interestingly, the lung and heart tissues at both sacrifice points obtained from the silver nanoparticles in either the prevented or treated groups exhibited mild to moderate histopathological changes, with preservation of the tissue architecture. Additionally, these nano-silver groups showed a significant reduction in the average histopathological lesion scores of the lungs and heart compared to the *E. coli* infected group. These results demonstrate the effectiveness of Ag NPs in reducing the severity of E. coli-induced lesions and suggest that Ag NPs have strong potential as an antimicrobial agent for controlling *E. coli* infection in both protective and therapeutic protocols. Several mechanisms have been proposed to explain the antibacterial effects of silver nanoparticles. The first mechanism involves the attachment of Ag NPs to the bacterial cell membrane. Positively charged Ag NPs can adhere to the negatively charged bacterial cell membrane (Dakal *et al.*, 2016). This electrostatic attraction can make Ag NPs interact with the bacterial cell membrane and cause detrimental changes to the integrity of the cell membrane, which can result in bacterial cell demise. Moreover, the studies using advanced microscopy techniques have demonstrated these changes including alterations to cell membrane structure that increasing the permeability of cell membrane, leading to disruption of the transport regulation (Raffi *et al.*, 2008), shrinking and rupture of cell membrane (Liao *et al.*, 2019), perforations in the cell membranes (Shrivastava *et al.*, 2007). All of these negative effects on the cell membrane can contribute to the transport of Ag NPs inside the bacterial cell. Meanwhile, the second mechanism is disrupting the intracellular structure and functions as Ag NPs can interact with the genetic material of bacteria, resulting in inhibition of the bacterial replication process (Morones *et al.*, 2005). Ag NPs can also disrupt the process of energy production in mitochondria. This disruption prevents the mitochondria from generating adenosine triphosphate (ATP) (Wypij *et al.*, 2020). Additionally, silver nanoparticles can suppress protein synthesis inside the bacterial cell through the same pathway used by some traditional antibiotics (Lara *et al.*, 2010). Moreover, many various essential enzymes can be deactivated by Ag NPs (Prabhu and Poulose, 2012). Together, these disruptions may lead to the dysfunction of bacterial organelles and ultimately result in bacterial cell death. The third proposed mechanism involves the ability of Ag NPs to induce oxidative stress within bacterial cells, ultimately leading to their death. Ag NPs enhance the production of reactive oxygen species (ROS), which increases oxidative stress levels. This elevated oxidative stress damages cellular components, resulting in bacterial cell demise (Quinteros *et al.*,

2016). Notably, chitosan, used in this study during the preparation of Ag NPs as both a reducing agent and stabilizer to prevent agglomeration, can also enhance the antibacterial effectiveness of Ag NPs. This combination may provide better efficacy than Ag NPs alone, as shown in results reported by Hassanen *et al.* (2021). Chitosan is non-toxic, biocompatible, and possesses antimicrobial properties. It is considered to have effective antimicrobial activity either alone or when combined with silver nanoparticles (Al-Zahrani *et al.*, 2021).

In our study, H and E staining and histopathological scoring of the lungs and heart in the ZnO QDs prevented and treated groups, revealing mild histopathological changes, with low average scores observed at both sacrifice points. These findings demonstrate the high efficacy of ZnO QDs in protecting and healing cardiopulmonary tissues from lesions induced by *E. coli* infection in poultry. This promising outcome can be attributed to the potent antibacterial activity of ZnO, which is size-dependent. ZnO QDs, being smaller, are more effective as antibacterial agents compared to larger nanoparticles or bulk ZnO. This small size plays an important role in allowing more Zinc oxide particles to attach to bacterial cell membranes, leading to an increased level of ROS and Zinc ions, which cause damaging effects to the stability of bacterial cells and eventually achieve a bactericidal effect (Singh *et al.*, 2018; Li *et al.*, 2021).

Conclusion

In conclusion, the histopathological findings underscore the severity of *colibacillosis* in poultry and the potential therapeutic benefits of metal nanoparticles, such as Ag NPs and ZnO QDs. Continued research into the mechanisms of action and clinical applications of these nanomaterials will be crucial in developing effective interventions to combat APEC infections and reduce the economic burden of this disease in the poultry industry.

Acknowledgement

We gratefully acknowledge the Department of Pathology,Faculty of Veterinary Medicine, Benha University, for their methodological guidance , technical support, and critical insights. Their expertise and collaborative environment were instrumental to the successful completion of this research.

Novelty Statement

This study is the first to demonstrate the in vivo efficacy of zinc oxide quantum dots (ZnO QDs) and chitosan-stabilized silver nanoparticles (Ag NPs) in both preventive and therapeutic roles against E. coli-induced cardiopulmonary lesions in broiler chicks, offering a novel nanotechnology-based alternative to combat antibiotic-resistant avian pathogens.

Author's Contribution

Mohammed Abdeldayem Mohammed Afifi: Methodology, writing original draft, writing review and editing.
Shawky Ahmed Moustafa: Supervision, writing review and editing, project administration.
Aziza Abd Elfattah Amin: Supervision, writing original draft, writing review and editing.
Sawsan Sami Mesalam El-Basuni: Methodology, writing original draft, writing review and editing.
Mohamed Mahmoud Salem Gaballa: Writing original draft, writing review and editing.

Conflict of interest
The authors have declared no conflict of interest.

References

Abd El-Ghany, W.A. and Madian, K., 2011. Control of experimental colisepticaemia in broiler chickens using sarafloxacin. Life Sci. J., 8(3): 318-328.

Abd El-Tawab, A.A., El-Komy, A.A., El-Ekhnawy, K.I. and Talaie, A.T., 2015. Effect of fosfomycin on *E. coli* O78 isolated from broiler chickens *in-vitro* and *in-vivo*. Benha Vet. Med. J., 28: 294-300. https://doi.org/10.21608/bvmj.2015.32501

Abreu, R., Semedo-Lemsaddek, T., Cunha, E., Tavares, L. and Oliveira, M., 2023. Antimicrobial drug resistance in poultry production: Current status and innovative strategies for bacterial control. Microorganisms, 11(4): 953. https://doi.org/10.3390/microorganisms11040953

Al-Zahrani, S.S., Bora, R.S. and Al-Garni, S.M., 2021. Antimicrobial activity of chitosan nanoparticles. Biotechnol. Biotechnol. Equip., 35(1): 1874-1880. https://doi.org/10.1080/131

02818.2022.2027816

Amen, O., El-Hendy, A.H., Elfeil, W.K. and Hussein, A.G., 2023. Evaluating the efficacy of commercial Escherichia coli killed vaccine in broiler chickens. J. Adv. Vet. Res., 13(6): 1037-1043.

Bancroft, J.D. and Layton, C., 2019. The hematoxylin and eosin. In: (eds. S.K. Suvarna, C. Layton and J.D. Bancroft), Bancroft's theory and practice of histological techniques, 8th Ed. Elsevier, Philadelphia, pp. 126–138. https://doi.org/10.1016/B978-0-7020-6864-5.00010-4

Bruna, T., Maldonado-Bravo, F., Jara, P. and Caro, N., 2021. Silver nanoparticles and their antibacterial applications. Int. J. Mol. Sci., 22(13): 7202. https://doi.org/10.3390/ijms22137202

Chen, J., Tang, Y.X., Kang, J.X., Xu, Y.R., Elsherbeni, A.I.A., Gharib, H.B.A. and Li, J.L., 2022. Astragalus polysaccharide alleviates transport stress-induced heart injury in newly hatched chicks via ERS-UPR-autophagy dependent pathway. Poult. Sci., 101(9): 102030. https://doi.org/10.1016/j.psj.2022.102030

Dakal, T.C., Kumar, A., Majumdar, R.S. and Yadav, V., 2016. Mechanistic basis of antimicrobial actions of silver nanoparticles. Front. Microbiol., 7: 1831. https://doi.org/10.3389/fmicb.2016.01831

Dziva, F. and Stevens, M.P., 2008. Colibacillosis in poultry: Unravelling the molecular basis of virulence of avian pathogenic *Escherichia coli* in their natural hosts. Avian Pathol., 37(4): 355-366. https://doi.org/10.1080/03079450802216652

El-Shaer, A., Awad, A. and Younis, G., 2023. Detection of carbapenem resistance mechanisms among avian pathogenic Escherichia coli (APEC) isolated from broiler chickens. J. Vet. Healthc., 3(1): 13.

Fatima, A., Zaheer, T., Pal, K., Abbas, R.Z., Akhtar, T., Ali, S. and Mahmood, M.S., 2024. Zinc oxide nanoparticles significant role in poultry and novel toxicological mechanisms. Biol. Trace Element. Res., 202(1): 268–290. https://doi.org/10.1007/s12011-023-03651-x

Gharpure, S. and Ankamwar, B., 2020. Synthesis and antimicrobial properties of zinc oxide nanoparticles. J. Nanosci. Nanotechnol., 20(10): 5977-5996. https://doi.org/10.1166/jnn.2020.18707

Guabiraba, R. and Schouler, C., 2015. Avian colibacillosis: Still many black holes. FEMS Microbiol. Lett., 362(15): fnv118. https://doi.org/10.1093/femsle/fnv118

Hassanen, E.I., Morsy, E.A., Hussien, A.M., Farroh, K.Y. and Ali, M.E., 2021. Comparative assessment of the bactericidal effect of nanoparticles of copper oxide, silver, and chitosan-silver against *Escherichia coli* infection in broilers. *Biosci. Rep.*, 41(4): BSR20204091. https://doi.org/10.1042/BSR20204091

Ibrahim, A.H., El-Khashab, E., Shakal, M. and Morsy, E.A., 2024. Unveiling antibiotic resistance, virulence, and molecular detection of enteric bacterial infections in broilers: A study in Egypt. Egypt. J. Vet. Sci., 55(6): 1537–1551. https://doi.org/10.21608/ejvs.2024.254290.1715

Jin, T., Sun, D., Su, J., Zhang, H.W. and Sue, H.J., 2009. Antimicrobial efficacy of zinc oxide quantum dots against *Listeria monocytogenes, Salmonella enteritidis,* and *Escherichia coli* O157: H7. J. Food Sci., 74(1): M46-M52. https://doi.org/10.1111/j.1750-3841.2008.01013.x

Lara, H.H., Ayala-Núnez, N.V., Ixtepan, T.L.D.C. and Rodríguez, P.C., 2010. Bactericidal effect of silver nanoparticles against multidrug-resistant bacteria. World J. Microbiol. Biotechnol., 26: 615–621. https://doi.org/10.1007/s11274-009-0211-3

Leitner, G. and Heller, E., 1992. Colonization of *Escherichia coli* in young turkeys and chickens. Avian Dis., 36(2): 211-220. https://doi.org/10.2307/1591493

Li, Y., Xie, S., Xu, D., Shu, G. and Wang, X., 2021. Antibacterial activity of ZnO quantum dots and its protective effects of chicks infected with *Salmonella pullorum.* Nanotechnology, 32(50): 505104. https://doi.org/10.1088/1361-6528/ac2846

Liao, S., Zhang, Y., Pan, X., Zhu, F., Jiang, C., Liu, Q., Cheng, Z., Dai, G., Wu, G. and Wang, L., 2019. Antibacterial activity and mechanism of silver nanoparticles against multidrug-resistant *Pseudomonas aeruginosa*. Int. J. Nanomed., 14: 1469-1487. https://doi.org/10.2147/IJN.S191340

Mateos-Hernández, L., Risco-Castillo, V., Torres-Maravilla, E., Bermúdez-Humarán, L.G., Alberdi, P., Hodžić, A., Hernández-Jarguin, A., Rakotobe, S., Galon, C. and Devillers, E., 2020. Gut microbiota abrogates anti-α-Gal

IgA response in lungs and protects against experimental Aspergillus infection in poultry. Vaccines, 8(2): 285. https://doi.org/10.3390/vaccines8020285

Mellata, M., 2013. Human and avian extraintestinal pathogenic *Escherichia coli*: Infections, zoonotic risks, and antibiotic resistance trends. Foodborne Pathog. Dis., 10(11): 916–932. https://doi.org/10.1089/fpd.2013.1533

Morones, J.R., Elechiguerra, J.L., Camacho, A., Holt, K., Kouri, J.B., Ramírez, J.T. and Yacaman, M.J., 2005. The bactericidal effect of silver nanoparticles. Nanotechnology, 16(10): 2346. https://doi.org/10.1088/0957-4484/16/10/059

Paudel, S., Fink, D., Abdelhamid, M.K., Zöggeler, A., Liebhart, D., Hess, M. and Hess, C., 2021. Aerosol is the optimal route of respiratory tract infection to induce pathological lesions of colibacillosis by a lux-tagged avian pathogenic *Escherichia coli* in chickens. Avian Pathol., 50(5): 417–426. https://doi.org/10.1080/03079457.2021.1978392

Pourbakhsh, S.A., Boulianne, M., Martineau-Doizé, B., Dozois, C.M., Desautels, C. and Fairbrother, J.M., 1997. Dynamics of *Escherichia coli* infection in experimentally inoculated chickens. Avian Dis., 41(1): 221–233. https://doi.org/10.2307/1592463

Prabhu, S. and Poulose, E.K., 2012. Silver nanoparticles: Mechanism of antimicrobial action, synthesis, medical applications, and toxicity effects. Int. Nano Lett., 2: 1–10. https://doi.org/10.1186/2228-5326-2-32

Quinteros, M., Aristizábal, V.C., Dalmasso, P.R., Paraje, M.G. and Páez, P.L., 2016. Oxidative stress generation of silver nanoparticles in three bacterial genera and its relationship with the antimicrobial activity. Toxicol. in vitro, 36: 216–223. https://doi.org/10.1016/j.tiv.2016.08.007

Raffi, M., Hussain, F., Bhatti, T., Akhter, J., Hameed, A. and Hasan, M., 2008. Antibacterial characterization of silver nanoparticles against *E. coli* ATCC-15224. J. Mater. Sci. Technol., 24(2): 192–196.

Shah, S.A., Mir, M.S., Wani, B.M., Kamil, S.A., Goswami, P., Amin, U., Shafi, M., Rather, M.A. and Beigh, A.B., 2019. Pathological studies on avian pathogenic *Escherichia coli* infection in broilers. Pharm. Innov. J., 8(7): 68–73.

Shrivastava, S., Bera, T., Roy, A., Singh, G., Ramachandrarao, P. and Dash, D., 2007. Retracted: Characterization of enhanced antibacterial effects of novel silver nanoparticles. Nanotechnology, 18(22): 225103. https://doi.org/10.1088/0957-4484/18/22/225103

Singh, A.K., Pal, P., Gupta, V., Yadav, T.P., Gupta, V. and Singh, S.P., 2018. Green synthesis, characterization and antimicrobial activity of zinc oxide quantum dots using *Eclipta alba*. Mater. Chem. Phys., 203: 40–48. https://doi.org/10.1016/j.matchemphys.2017.09.049

Singh, P., Sood, S., Nashiruddullah, N., Rahman, S., Gupta, P. and Sharma, S., 2024. Colibacillosis associated spontaneously occurring respiratory tract lesions in broilers of Jammu. Haryana Vet., 63(SI): 70–75.

Stordeur, P., Marlier, D., Blanco, J., Oswald, E., Biet, F., Dho-Moulin, M. and Mainil, J., 2002. Examination of *Escherichia coli* from poultry for selected adhesin genes important in disease caused by mammalian pathogenic *E. coli*. Vet. Microbiol., 84(3): 231-241. https://doi.org/10.1016/S0378-1135(01)00464-3

Wei, D., Sun, W., Qian, W., Ye, Y. and Ma, X., 2009. The synthesis of chitosan-based silver nanoparticles and their antibacterial activity. Carbohyd. Res., 344(17): 2375–2382. https://doi.org/10.1016/j.carres.2009.09.001

Wypij, M., Jędrzejewski, T., Ostrowski, M., Trzcińska, J., Rai, M. and Golińska, P., 2020. Biogenic silver nanoparticles: Assessment of their cytotoxicity, genotoxicity and study of capping proteins. Molecules, 25(13): 3022. https://doi.org/10.3390/molecules25133022